A novel Wnt/β-catenin signaling driven adipocyte population that is required for beiging

Zhi Liu[1,2,*], Tian Chen[1,2*], Sicheng Zhang[1,2], Tianfang Yang[1], Yun Gong[3], Hong-Wen Deng[3], Ding Bai[2], Weidong Tian[2¶], YiPing Chen[1¶]

[1]Department of Cell and Molecular Biology, Tulane University, New Orleans, LA, USA

[2]State Key Laboratory of Oral Diseases, National Clinical Research Center for Oral Disease, West China Hospital of Stomatology, Sichuan University, Chengdu, Sichuan Province, China

[3]Tulane Center of Biomedical Informatics and Genomic, Deming Department of Medicine, School of Medicine, Tulane University, New Orleans, LA, USA

[*]These authors contributed equally.

[¶]Corresponding authors: drtwd@sina.com; ychen@tulane.edu

Wnt/β-catenin signaling has been well established as a potent inhibitor of adipogenesis. Here, we identified a novel population of Wnt/β-catenin signaling driven adipocytes in embryonic and adult mouse fat depots. We showed that the activation of Wnt/β-catenin signaling in these cells relies on Akt/mTOR signaling intracellularly and is essential for cell survival. Such adipocytes are distinct from classic ones in transcriptomic and genomic signatures and can be induced from various sources of mesenchymal stromal cells including human bone marrow stromal cells. These adipocytes not only convert into beige adipocytes directly but are also required for beige adipocyte recruitment under thermal challenge, demonstrating a central role in initiating adaptive thermogenesis. Our studies shed new insights into adipocyte diversity and regulatory mechanism of beiging in adipose tissues.

Adipose tissues, consisting of white adipose tissue (WAT) and brown adipose tissue (BAT), play a critical role in maintaining whole-body metabolic homeostasis, with WAT serving for energy storage and BAT for energy dissipation to produce heat[1]. In addition to white and brown fat cells that are differentiated from heterogenous progenitors of distinct lineages[2,3], a third type of inducible adipocyte exists known as beige adipocytes that are transiently generated in WAT depots in response to external stimulations[4,5]. Like brown adipocytes, activated beige adipocytes express key thermogenic protein UCP1 and exert adaptive thermogenic function[6,7]. It is generally accepted that beige adipocytes arise by both de novo adipogenesis from progenitor cells and direct conversion/transdifferentiation from white adipocytes[8-10]. While previous studies have identified specific markers (for example, CD137 and CD81) for progenitors of beige adipocytes[11,12], the cellular origin of beige adipocytes derived from direct conversion and the regulatory mechanism of beiging remain elusive.

Wnt/β-catenin signaling pathway plays a fundamental role in cell proliferation, differentiation, and tissue homeostasis. In the presence of Wnts, cytoplasmic β-catenin translocates into the nucleus and interacts with TCF/LEF transcription factors to activate downstream target genes[13]. In addition, β-catenin nuclear translocation can also be triggered by other intracellular factors such as Akt and $G\alpha_s$, leading to the activation of Wnt/β-catenin signaling in a ligand- and receptor-independent manner[14,15]. Despite the consensus that Wnt/β-catenin signaling imposes negative effects on adipogenesis by inhibiting Pparγ[16-18], clues have been pointing to potential roles of Wnt/β-catenin signaling in adipogenesis and adipose function[19-21]. However, direct evidence is lacking.

In a survey for the presence of active Wnt/β-catenin signaling in any developing and mature adipocytes, we examined Wnt/β-catenin activity in various adipose depots in mice at different ages including embryonic stages. We took advantage of the Wnt/β-catenin signaling specific reporter mouse line *TCF/Lef:H2B-GFP* (hereafter *T/L-GFP*) that allows real-time monitoring of Wnt/β-catenin activity at single-cell resolution[22]. Surprisingly, we virtually observed a subset of Perilipin$^+$ adipocytes that exhibited Wnt/β-catenin signaling activity interspersed within various fat depots, including interscapular BAT (iBAT), inguinal WAT (iWAT), epididymal WAT (eWAT), and bone marrow (BM) in both male and female adult mice (Fig. 1A and Supplemental Fig. 2, A and B). To confirm that these Wnt/β-catenin positive cells are indeed adipocytes, we created a *Tcf/Lef-CreERT2* transgenic allele in which the *CreERT2* cassette was placed under the control of the same regulatory elements as that used in the *T/L-GFP* allele (Supplemental Fig. 1A and Methods). This *Tcf/Lef-CreERT2* allele indelibly labeled the cell membrane of adipocytes upon compounding with *Rosa26R*^{mTmG} reporter allele followed by tamoxifen administration and exhibited overlapped expression with *T/L-GFP* allele in fat tissues (Supplemental Fig. 1, B-D). This population of fat cell was referred as Wnt$^+$ adipocytes accordingly, which count for various

percentages of total fat cells in different fat depots, with the highest level (17.02% ± 3.06%) seen in iBAT and the lowest one (1.28% ± 0.56%) in eWAT of adult male mice (Fig. 1B). However, in fat depots in females, the percentage of Wnt^+ adipocyte is around half as compared to their male counterparts (Supplemental Fig. 2, A and B). Wnt^+ adipocytes could be detected as early as embryonic day 17.5 (E17.5) and its percentage varied in different fat depots as mice aged (Supplemental Fig. 2, C-F). By standard white fat pro-adipogenic induction (Methods), we readily induced Wnt^+ adipocytes, as confirmed by staining of Pparγ and Adiponectin (Fig. 1D), from stromal vascular fraction (SVF) cells derived from iBAT, iWAT, eWAT, as well as BM stroma, with similar morphology as compared to Wnt^- (non-GFP labeled) adipocytes (Fig. 1A). Induced Wnt^+ adipocytes also made up a similar percentage of total induced fat cells as they are present in their corresponding fat depot (Fig. 1C). The fact that E13.5 mouse embryonic fibroblasts (MEFs) could also differentiate into Wnt^+ adipocytes in vitro (Supplemental Fig. 2G) suggested an early developmental origin of Wnt^+ adipocytes. Importantly, we were able to induce Wnt^+ adipocytes from human primary bone marrow stromal cells (BMSCs) carrying a *TCF/Lef:H2B-GFP* reporter cassette (Fig. 1E, Supplemental Fig. 3, and Methods), implicating the presence of Wnt^+ adipocytes in humans.

To address how Wnt^+ adipocytes develop during adipogenesis, we conducted real-time monitoring on induced Wnt^+ adipocytes in vitro. No Wnt/β-catenin signaling activity was seen in precursors prior to pro-adipogenic induction (Supplemental Fig. 4A). Wnt/β-catenin signaling activity was initially detected in differentiated adipocytes (defined by the presence of lipid droplets) after 2-day adipogenic induction and could be sustained once activated (Supplemental Fig. 4A), indicating that Wnt/β-catenin signaling does not transiently appear but persists in Wnt^+ adipocytes. After 7-day differentiation, we observed colonized Wnt^+ and Wnt^- adipocytes, suggesting distinct cell lineages of these two different

populations of adipocytes (Supplemental Fig. 4B). This conclusion is supported by the observation that induced Wnt^+ and Wnt^- adipocytes, after separation by fluorescence-activated cell sorting (FACS) and subsequent 4-day in culture, did not convert mutually (Fig. 2A).

To ensure that the GFP expression in fat depots and adipocytes induced from precursors of *T/L-GFP* mice represents true Wnt/β-catenin signaling activity, we first confirmed the presence of active β-catenin and Tcf/Lef1 in the nuclei of Wnt^+ adipocytes within adipose tissues (Supplemental Fig. 4, C and D). We found that Tcf4 (also known as Tcf7l2) expression was largely overlapped with Wnt^+ adipocytes (Supplemental Fig. 4D), whereas other Tcf proteins (Tcf1, Lef1, and Tcf3) were barely seen in Wnt^+ adipocytes (data not shown). To determine if inhibition of Wnt/β-catenin signaling would diminish GFP in Wnt^+ adipocytes, we conducted knockdown experiments using short interfering RNA (siRNA) targeting *Ctnnb1* (encoding β-catenin) followed by real-time monitoring (Methods). As shown in Figure 2B, *Ctnnb1* knockdown in differentiated Wnt^+ adipocytes indeed quenched GFP signals. Interestingly, DKK1 and IWP-2, both canonical Wnt receptor antagonists, failed to, but LF3, a molecule that disrupts the interaction between β-catenin and Tcf4[23], did inhibit Wnt/β-catenin signaling activity in precursors under pro-adipogenic conditions (Fig. 2C and Supplemental Fig. 4, E-G), indicating that the activation of Wnt/β-catenin signaling in Wnt^+ adipocytes is ligand- and receptor-independent. Moreover, LF3 treatment not only resulted in paucity of Wnt^+ adipocytes but also an overall impaired/delayed adipogenic maturation of SVF-derived adipocytes in a dose-dependent manner (Fig. 2C), suggesting a potential functional importance of the intracellular Wnt/β-catenin signaling in adipogenesis. To further define the role of Wnt/β-catenin signaling in Wnt^+ and Wnt^-adipocytes, we established an immortalized SVF cell line (mBaSVF) derived from iBAT of *T/L-GFP* mouse (Methods). By serial limited dilutions, we

isolated two Wnt$^+$ and two Wnt$^-$ adipocyte precursor cell lines from mBaSVF cells (GFPpos-1, GFPpos-2, GFPneg-1, and GFPneg-2 cells), respectively. LF3 treatment of induced Wnt$^+$ adipocytes from both GFPpos-1 and GFPpos-2 cell lines caused quenching of GFP signals first, followed by massive cell death (Supplemental Fig. 5, A-D). By contrast, LF3 administration to induced Wnt$^-$ adipocytes from precursor cell lines did not affect cell viability but slowed down maturation of Wnt$^-$ adipocytes (Supplemental Fig. 5, A, and D-F), similar to that seen in SVF induced adipocytes (Fig. 2C). However, such LF3-treated Wnt$^-$ adipocytes, once returned to normal pro-adipogenic medium, resumed full adipogenic capacity compared to controls (Supplemental Fig. 5, G-H), indicating that LF3 treatment does not impair but delays maturation of Wnt$^-$ adipocytes. As controls, the same dose of LF3 showed no impacts on uninduced Wnt$^+$ and Wnt$^-$ precursor cell lines (Supplemental Fig. 6G).

Akt/mTOR signaling modulated by insulin promotes cytoplasmic β-catenin accumulation through GSK-3β phosphorylation[24,25]. To test if Akt/mTOR signaling is responsible for intracellular Wnt/β-catenin signaling activation in Wnt$^+$ adipocytes, we treated iBAT-derived SVF cells under pro-adipogenic conditions with LY294002, a selective Akt signaling antagonist. Again, we found a dramatically reduced number of Wnt$^+$ adipocytes and delayed adipogenesis in a dose-dependent manner (Supplemental Fig. 6, A and B). Consistently, LY294002 administration to Wnt$^+$ adipocytes induced from precursor cell lines eliminated GFP signals and caused massive cell death as well (Supplemental Fig. 6, C-G). We further subjected *T/L-GFP* adult mice to an mTOR-specific antagonist Temsirolimus treatment (Methods), which dramatically reduced Wnt$^+$ adipocyte number in iWAT and iBAT compared to vehicle-injected controls (Fig. 2, D and E). These results show that the activation of the intracellular Wnt/β-catenin signaling in Wnt$^+$ adipocytes depends on active Akt/mTOR signaling, which is required for cell survival.

To further distinguish Wnt$^+$ adipocytes from Wnt$^-$ fat cells and explore the global diversity at molecular and genomic levels, we performed single-cell RNA sequencing analysis (scRNA-seq) and single-cell assay for transposase-accessible chromatin sequencing (scATAC-seq) on FACS separated Wnt$^+$ and Wnt$^-$ adipocytes induced from iWAT- and iBAT-derived SVF cells, respectively (Fig. 3A and Methods). After filtering for quality and excluding non-adipocytes (Methods), bioinformatic analyses classified the input Wnt$^+$ and Wnt$^-$ adipocytes into distinct clusters, indicating two different types of adipocytes (Fig. 3, B and C, Supplemental Fig. 7A, and Supplemental Fig. 8). Notably, although the mRNA expression of *Ucp1* was undetectable, several thermogenic genes such as *Cox8b*, *Elovl3*, and *Cidea* were found at significantly higher levels in Wnt$^+$ adipocytes without browning stimulation (Fig. 3, D and E, and Supplemental Fig. 7, B and C), indicative of thermogenic character. Moreover, *Cyp2e1*, identified as a marker gene in thermogenic regulation[26], and *Cidea* were exclusively expressed in a subset of Wnt$^+$ adipocytes induced from iWAT- and iBAT-derived SVFs, as confirmed by immunofluorescent staining (Fig. 3D and Supplemental Fig. 7, D and E). These facts link Wnt$^+$ adipocytes to thermogenic function in adipose tissues. Enrichment analysis of significantly differentially expressed genes (DEGs) also suggests the primary functions of this population of adipocytes in the regulation of adipogenesis, fatty acid metabolism, xenobiotic metabolism, glycolysis, and mTORC1 signaling (Supplemental Fig. 7, F-I). These results demonstrated that this novel population of Wnt/β-catenin signaling driven adipocytes is distinct from the classic adipocytes at molecular and genomic levels and is implicated in thermogenic metabolism.

The potential higher metabolic and thermogenic characters in Wnt$^+$ adipocytes prompted us to investigate the adaptive thermogenic role of Wnt$^+$ adipocytes. We first examined mitochondrial activities in Wnt$^+$ and Wnt$^-$ adipocytes induced from SVFs. As shown in Figure 4A and 4B, Wnt$^+$ adipocytes, along with those closely adjacent Wnt$^-$ fat

cells, exhibited pronounced lower levels of mitochondrial membrane potential, indicative of higher uncoupling rate, as compared to those Wnt$^-$ fat cells located relatively away from Wnt$^+$ adipocytes. In addition, significant higher levels of oxygen consumption rate (OCR) were detected in Wnt$^+$ adipocytes induced from precursor cell lines as compared to those induced from mBaSVF and Wnt$^-$ precursor cell lines (Fig. 4C and Supplemental Fig. 9, A and B), further demonstrating a higher mitochondrial respiration capacity of Wnt$^+$ adipocytes. To explore the possible involvement of Wnt$^+$ adipocyte in adaptive thermogenesis in vivo, adult *T/L-GFP* male mice were subjected to 6ºC for 2-day. After cold exposure, a subset of UCP1-expressing beige adipocytes was also Wnt-positive (Fig. 4D), demonstrating that a portion of beige fat cells arises from Wnt$^+$ adipocyte lineage. Similar results were seen in mice treated with β3-adrenergic receptor agonist CL316,243 (Supplemental Fig. 9C and Methods). Interestingly, the total number of Wnt+ adipocytes in iWAT did not change in response to cold stress or β3-adrenergic receptor agonist treatments, compared to controls (Supplemental Fig. 9D). Notably, the majority of, if not all, UCP1-labeled beige adipocytes were found closely adjacent to Wnt$^+$ adipocytes (Fig. 4D), implicating a regulatory role of Wnt$^+$ adipocytes in beige fat biogenesis. As cold exposure was prolonged to 4-day, abundant beige adipocytes were present in close approximation to Wnt$^+$ adipocytes. Again, beige adipocytes were rarely seen away from Wnt$^+$ adipocytes (Supplemental Fig. 9E). Together with the results from mitochondrial activity assays, these observations suggest a paracrine function of Wnt$^+$ adipocytes.

To further establish a critical role for Wnt$^+$ adipocytes in beiging, we conducted lineage-tracing studies using *Tcf/Lef-CreERT2*;*Rosa26R*^{mTmG} mice, which, after 4-day cold acclimation at 6ºC following tamoxifen administration, manifested the presence of mGFP and UCP1 co-labeled adipocytes in iWAT (Fig. 4E and Methods). This result provides unambiguous evidence for direct conversion of Wnt$^+$ adipocytes into beige fat cells. To

investigate the paracrine function of Wnt$^+$ adipocytes in beige fat biogenesis, we generated a *Fabp4-Flex-DTA* mouse model (Supplemental Fig. 9F and Methods), which allowed targeted ablation of Wnt$^+$ adipocytes after crossing to *Tcf/Lef-CreERT2* mice and followed by tamoxifen administration (Supplemental Fig. 9G). After 2-day cold stress, diphtheria-toxin-induced depletion of Wnt$^+$ adipocytes led to substantially reduced beige adipocytes (Fig. 4F), verified by remarkably decreased expression levels of thermogenic genes (Fig. 4G). These results demonstrate an essential role of Wnt$^+$ adipocytes in initiating beige adipogenesis under acute cold conditions via non-cell autonomous effect.

While numerous studies support the notion that Wnt/β-catenin signaling suppresses adipogenesis[16-18], our current studies present direct evidence for the existence of a population of intracellular Wnt/β-catenin signaling driven adipocytes, revealing the diversity of adipocytes. Our results show that the intracellular Wnt/β-catenin signaling is not only essential for the survival of Wnt$^+$ adipocyte but is also required for normal maturation of Wnt$^-$ adipocytes, though the underlying mechanisms warrant further investigation. Since Akt/mTOR signaling is known to promote lipid accumulation and is required for the activation of the intracellular Wnt/β-catenin signaling, it is possible that Wnt$^-$ adipocytes also possess basal activity of Wnt/β-catenin signaling that is required for lipid accumulation. This hypothesis is consistent with a prior study that silencing *Tcf7l2* leads to blockade of adipogenesis[19].

Our studies have also uncovered a key role of Wnt$^+$ adipocytes in adaptive thermogenesis of adipose tissues. Wnt$^+$ adipocytes represent at least one of the cell populations that can convert into beige adipocytes directly following cold stress. Notably, Wnt$^+$ adipocytes are also required for beige adipogenesis. Wnt$^+$ adipocytes act as a key initiator in beige biogenesis through both cell autonomous (direct conversion) and non-autonomous (recruitment) manners. Since thermogenic adipocytes are proven to protect

against diet-induced obesity and metabolic disorders[27-30], and GWAS has also linked genetic variation in *TCF7L2* to type 2 diabetes in humans[19,31], it is conceivable that the Wnt$^+$ adipocytes are a population of beneficial adipocytes to regulate whole-body metabolic homeostasis. The evidence that Wnt$^+$ adipocytes could be induced from human primary BMSCs opens a door for translational research in the near future.

Acknowledgements: We thank members of the Chen Lab for providing technical advice and sharing reagents. This work was supported by a Carol Lavin Bernick Faculty Grant from Tulane University and the John L. and Mary Wright Ebaugh Endowed Chair Fund (Y.C.). Z.L., T.C. and S.Z. each were supported in part by fellowship from China Scholarship Council. T.Y. was supported by an American Heart Association Predoctoral Fellowship (20PRE35040002).

Author Contributions: Z.L., T.C., W.T. and Y.C. conceived the study and designed experiments. D.B. helped to design the initial experiments and provide mentoring and intellectual advice during the study. Z.L., T.C., S.Z., T.Y. performed experiments. Y.G. and H.D. helped to analyze bioinformatic data. Z.L., T.C., S.Z., W.T. and Y.C. collected, analyzed, and interpreted data. Z.L. and T.C. wrote manuscript, and Z.L., T.C., W.T. and Y.C edited the manuscript.

Competing interests: Y.C., Z.L., T.C. and S.Z. are inventors on a provisional patent application related to this work filed by Tulane University (NO. 63126170), on December 16, 2020. The authors declare no competing interests.

Data and materials availability: The GEO accession number for the scRNA-seq and scATAC-seq data is GSE164747 and additional details regarding analytics are available at https://github.com/ychen-lab/Wnt-positive-adipocyte. Transgenic mice and precursor cell

lines generated in the Chen Lab and used in this study will be available for research use only upon request.

Reference

1 Ross, S. E. *et al.* Inhibition of adipogenesis by Wnt signaling. *Science* **289**, 950-953, doi:10.1126/science.289.5481.950 (2000).

2 Waki, H. *et al.* The small molecule harmine is an antidiabetic cell-type-specific regulator of PPARgamma expression. *Cell Metab* **5**, 357-370, doi:10.1016/j.cmet.2007.03.010 (2007).

3 Longo, K. A. *et al.* Wnt10b inhibits development of white and brown adipose tissues. *J Biol Chem* **279**, 35503-35509, doi:10.1074/jbc.M402937200 (2004).

4 Chen, X. *et al.* The Diabetes Gene and Wnt Pathway Effector TCF7L2 Regulates Adipocyte Development and Function. *Diabetes* **67**, 554-568, doi:10.2337/db17-0318 (2018).

5 Geoghegan, G. *et al.* Targeted deletion of Tcf7l2 in adipocytes promotes adipocyte hypertrophy and impaired glucose metabolism. *Mol Metab* **24**, 44-63, doi:10.1016/j.molmet.2019.03.003 (2019).

6 Chen, M. *et al.* CTNNB1/beta-catenin dysfunction contributes to adiposity by regulating the cross-talk of mature adipocytes and preadipocytes. *Sci Adv* **6**, eaax9605, doi:10.1126/sciadv.aax9605 (2020).

7 Rosen, E. D. & Spiegelman, B. M. What we talk about when we talk about fat. *Cell* **156**, 20-44, doi:10.1016/j.cell.2013.12.012 (2014).

8 Schwalie, P. C. *et al.* A stromal cell population that inhibits adipogenesis in mammalian fat depots. *Nature* **559**, 103-108, doi:10.1038/s41586-018-0226-8 (2018).

9 Hepler, C., Vishvanath, L. & Gupta, R. K. Sorting out adipocyte precursors and their role in physiology and disease. *Genes Dev* **31**, 127-140, doi:10.1101/gad.293704.116 (2017).

10 Ikeda, K., Maretich, P. & Kajimura, S. The Common and Distinct Features of Brown and Beige Adipocytes. *Trends Endocrinol Metab* **29**, 191-200, doi:10.1016/j.tem.2018.01.001 (2018).

11 Bostrom, P. *et al.* A PGC1-alpha-dependent myokine that drives brown-fat-like development of white fat and thermogenesis. *Nature* **481**, 463-468, doi:10.1038/nature10777 (2012).

12 Ishibashi, J. & Seale, P. Medicine. Beige can be slimming. *Science* **328**, 1113-1114, doi:10.1126/science.1190816 (2010).

13 Petrovic, N. *et al.* Chronic peroxisome proliferator-activated receptor gamma (PPARgamma) activation of epididymally derived white adipocyte cultures reveals a population of thermogenically competent, UCP1-containing adipocytes molecularly distinct from classic brown adipocytes. *J Biol Chem* **285**, 7153-7164, doi:10.1074/jbc.M109.053942 (2010).

14 Wang, Q. A., Tao, C., Gupta, R. K. & Scherer, P. E. Tracking adipogenesis during white adipose tissue development, expansion and regeneration. *Nat Med* **19**, 1338-1344, doi:10.1038/nm.3324 (2013).

15 Shao, M. *et al.* Cellular Origins of Beige Fat Cells Revisited. *Diabetes* **68**, 1874-1885, doi:10.2337/db19-0308 (2019).

16 Barbatelli, G. *et al.* The emergence of cold-induced brown adipocytes in mouse white fat depots is determined predominantly by white to brown adipocyte transdifferentiation. *Am J Physiol Endocrinol Metab* **298**, E1244-1253, doi:10.1152/ajpendo.00600.2009 (2010).

17 Wu, J. *et al.* Beige adipocytes are a distinct type of thermogenic fat cell in mouse and human. *Cell* **150**, 366-376, doi:10.1016/j.cell.2012.05.016 (2012).

18 Oguri, Y. *et al.* CD81 Controls Beige Fat Progenitor Cell Growth and Energy Balance via FAK Signaling. *Cell* **182**, 563-577 e520, doi:10.1016/j.cell.2020.06.021 (2020).

19 Dale, T. C. Signal transduction by the Wnt family of ligands. *Biochem J* **329 (Pt 2)**, 209-223, doi:10.1042/bj3290209 (1998).

20 Fang, D. *et al.* Phosphorylation of beta-catenin by AKT promotes beta-catenin transcriptional activity. *J Biol Chem* **282**, 11221-11229, doi:10.1074/jbc.M611871200 (2007).

21 Regard, J. B. *et al.* Wnt/beta-catenin signaling is differentially regulated by Galpha proteins and contributes to fibrous dysplasia. *Proc Natl Acad Sci U S A* **108**, 20101-20106, doi:10.1073/pnas.1114656108 (2011).
22 Ferrer-Vaquer, A. *et al.* A sensitive and bright single-cell resolution live imaging reporter of Wnt/ss-catenin signaling in the mouse. *BMC Dev Biol* **10**, 121, doi:10.1186/1471-213X-10-121 (2010).
23 Fang, L. *et al.* A Small-Molecule Antagonist of the beta-Catenin/TCF4 Interaction Blocks the Self-Renewal of Cancer Stem Cells and Suppresses Tumorigenesis. *Cancer Res* **76**, 891-901, doi:10.1158/0008-5472.CAN-15-1519 (2016).
24 Schakman, O. *et al.* Role of Akt/GSK-3beta/beta-catenin transduction pathway in the muscle anti-atrophy action of insulin-like growth factor-I in glucocorticoid-treated rats. *Endocrinology* **149**, 3900-3908, doi:10.1210/en.2008-0439 (2008).
25 Hermida, M. A., Dinesh Kumar, J. & Leslie, N. R. GSK3 and its interactions with the PI3K/AKT/mTOR signalling network. *Adv Biol Regul* **65**, 5-15, doi:10.1016/j.jbior.2017.06.003 (2017).
26 Sun, W. *et al.* snRNA-seq reveals a subpopulation of adipocytes that regulates thermogenesis. *Nature* **587**, 98-102, doi:10.1038/s41586-020-2856-x (2020).
27 Tseng, Y. H., Cypess, A. M. & Kahn, C. R. Cellular bioenergetics as a target for obesity therapy. *Nat Rev Drug Discov* **9**, 465-482, doi:10.1038/nrd3138 (2010).
28 Lowell, B. B. *et al.* Development of obesity in transgenic mice after genetic ablation of brown adipose tissue. *Nature* **366**, 740-742, doi:10.1038/366740a0 (1993).
29 Crane, J. D. *et al.* Inhibiting peripheral serotonin synthesis reduces obesity and metabolic dysfunction by promoting brown adipose tissue thermogenesis. *Nat Med* **21**, 166-172, doi:10.1038/nm.3766 (2015).
30 Bartelt, A. & Heeren, J. Adipose tissue browning and metabolic health. *Nat Rev Endocrinol* **10**, 24-36, doi:10.1038/nrendo.2013.204 (2014).
31 Voight, B. F. *et al.* Twelve type 2 diabetes susceptibility loci identified through large-scale association analysis. *Nat Genet* **42**, 579-589, doi:10.1038/ng.609 (2010).

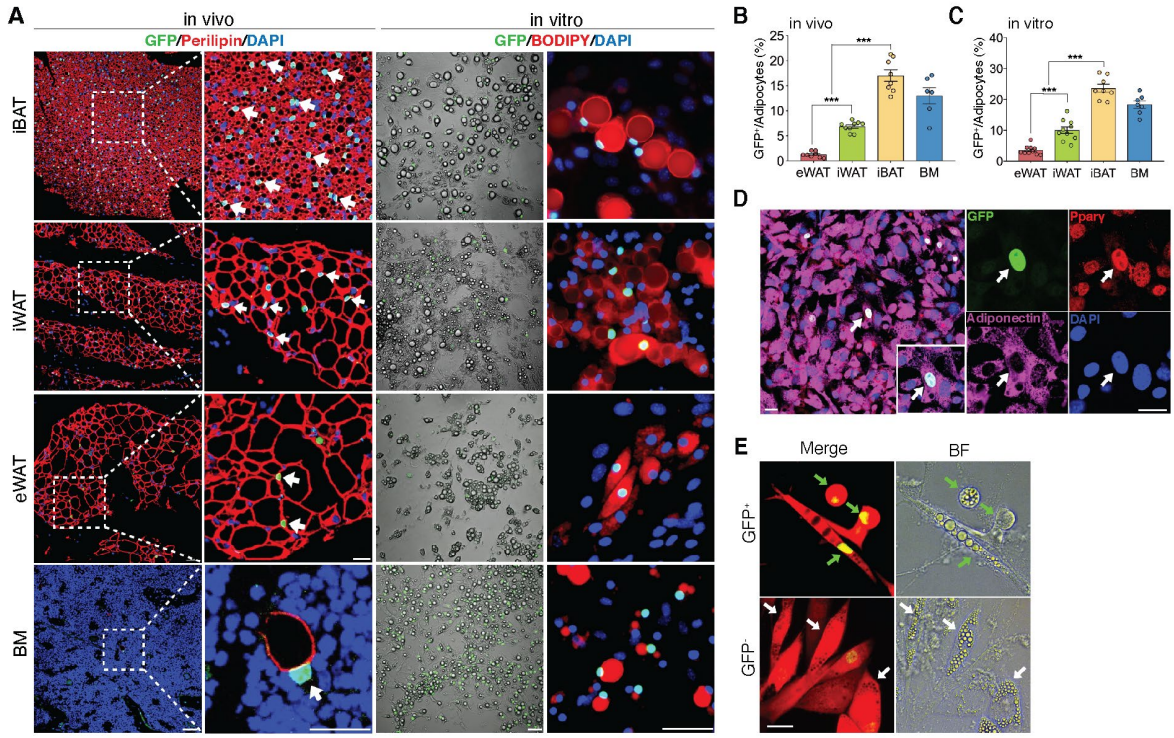

Fig. 1. The existence of adipocytes exhibiting active Wnt/β-catenin signaling. (**A**) Immunofluorescent and microscopy images of active Wnt/β-catenin signaling, indicated by GFP expression from the *TCF/Lef:H2B-GFP* allele, in adipocytes marked by Perilipin or BODIPY. Scale bars, 50 μm; close-up scale bars, 20 μm. (**B**) Quantification of Wnt^+ adipocytes among total adipocytes in various fat depots of adult male mice. Data are mean ± s.e.m., one-way ANOVA followed by Tukey's test; n = 6-9 mice; ***$P < 0.001$. (**C**) Quantification of Wnt^+ adipocytes among total adipocytes induced from SVF cells derived from adult male fat depots and BM stroma. Data are mean ± s.e.m., one-way ANOVA followed by Tukey's test; n = 7-10 independent experiments; ***$P < 0.001$. (**D**) Immunofluorescent staining of Pparγ and Adiponectin in cultured GFP^+ adipocytes derived from bone marrow of mice in (A). n = 3 independent experiments. Scale bars, 20 μm. (**E**) Representative images of GFP^+ (green arrows) and GFP^- (white arrows) adipocytes induced from human bone marrow stromal cells infected with *TCF/Lef:H2B-GFP* reporter lentiviral virus. n = 2 independent experiments, 3 independent wells each. Scale bar, 20 μm.

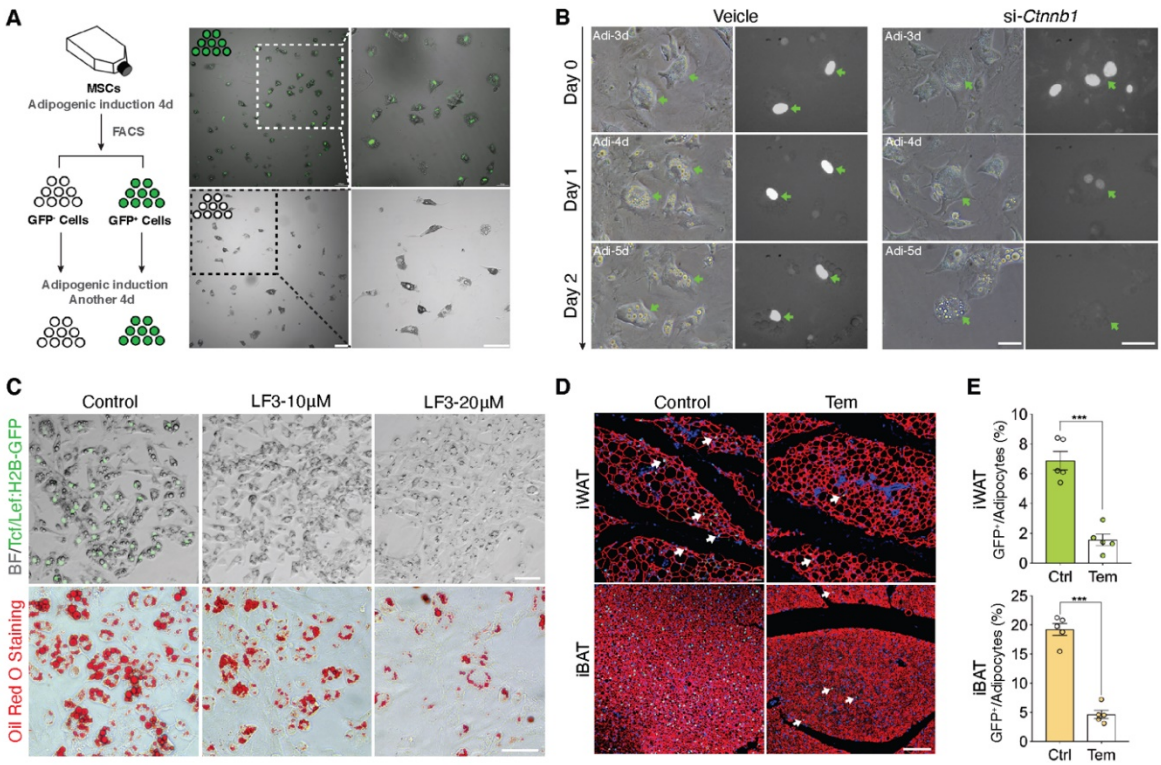

Fig. 2. Characterization of mouse Wnt⁺ adipocytes. (**A**) Schematic of the experiments and microscopy images of separated Wnt⁺ and Wnt⁻ adipocytes by FACS. $n = 3$ independent experiments. Scale bars, 100 μm. (**B**) Time-lapse microscopy images of induced Wnt⁺ adipocytes from BMSCs of *T/L-GFP* mice with *Ctnnb1* and control siRNA-mediated knockdown. $n = 2$ independent experiments, 3 independent wells each. Scale bars, 50 μm. (**C**) Microscopy images and Oil Red O staining of Wnt⁺ adipocytes induced from iBAT-derived SVF cells of *T/L-GFP* mice with control and LF3 treatment in different doses. $n = 5$ independent experiments. Scale bars, 50 μm. (**D**) Immunofluorescent images of iWAT and iBAT of *T/L-GFP* mice treated with or without Temsirolimus. $n = 5$ mice. Scale bar, 100 μm. (**E**) Quantification of Wnt⁺ adipocytes among total adipocytes in (D). Data are mean ± s.e.m., unpaired Student's *t*-test; ***$P < 0.001$.

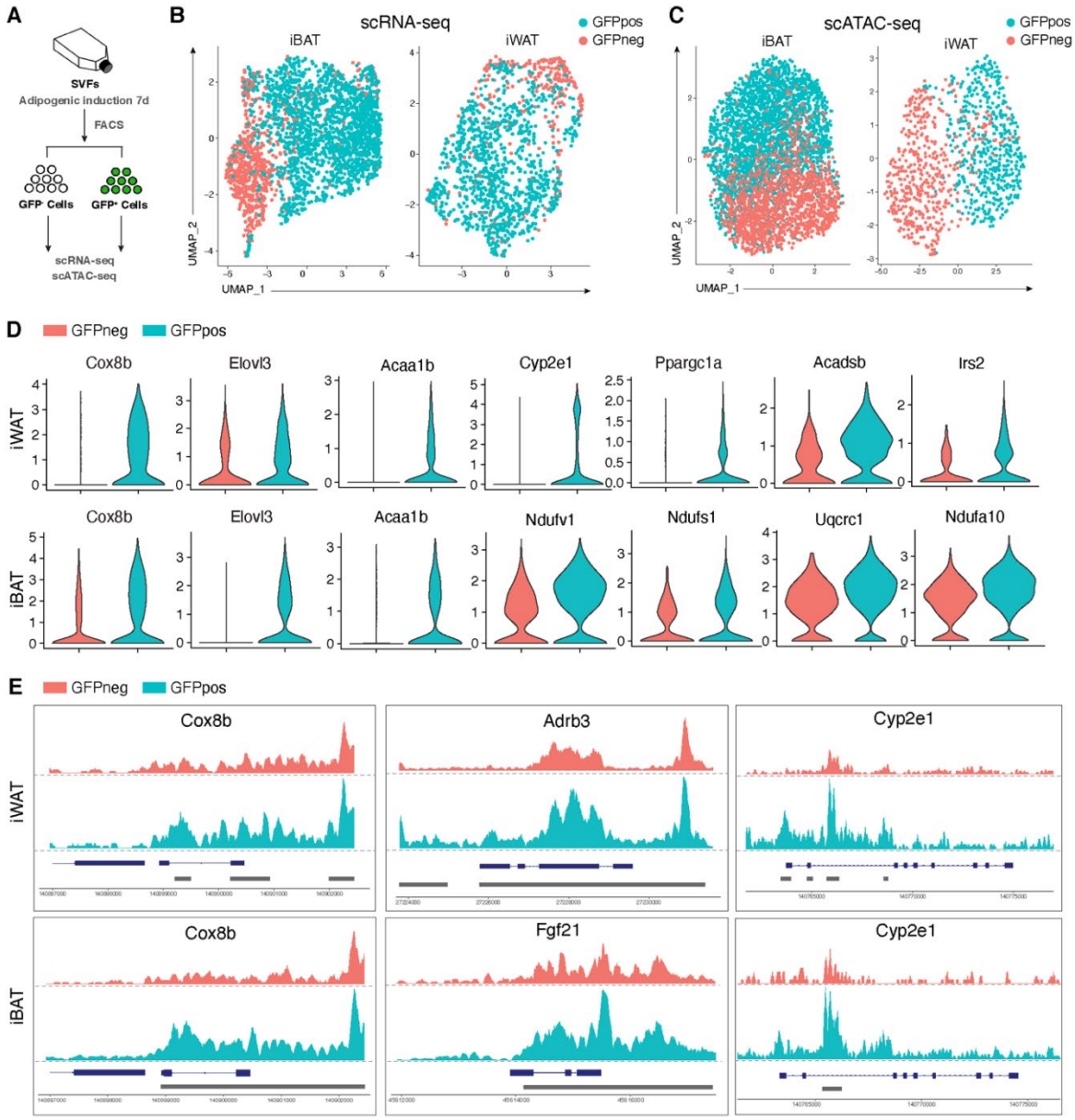

Fig. 3. Distinct molecular and genomic signatures of Wnt$^+$ and Wnt$^-$ adipocytes. (**A**) Schematic of scRNA-seq and scATAC-seq experiments from induced SVF cells. (**B**) Uniform Manifold Approximation and Projection (UMAP) visualization of 2,537 adipocytes from iBAT (1,710 GFP$^+$ and 827 GFP$^-$) and 1,345 adipocytes from iWAT (984 GFP$^+$ and 361 GFP$^-$) in scRNA-seq. (**C**) UMAP visualization of 4,302 adipocytes from iBAT (1,727 GFP$^+$ and 2,575 GFP$^-$) and 1,383 adipocytes from iWAT (562 GFP$^+$ and 821 GFP$^-$) in scATAC-seq. (**D**) Violin plots of induced Wnt$^+$ and Wnt$^-$ adipocytes showing the distribution of normalized expression values of indicated genes in scRNA-seq. (**E**) ScATAC-seq tracks of induced Wnt$^+$ and Wnt$^-$ adipocytes showing distinct chromatin accessibilities of indicated genes. GFPneg: Wnt$^-$ adipocytes; GFPpos: Wnt$^+$ adipocytes.

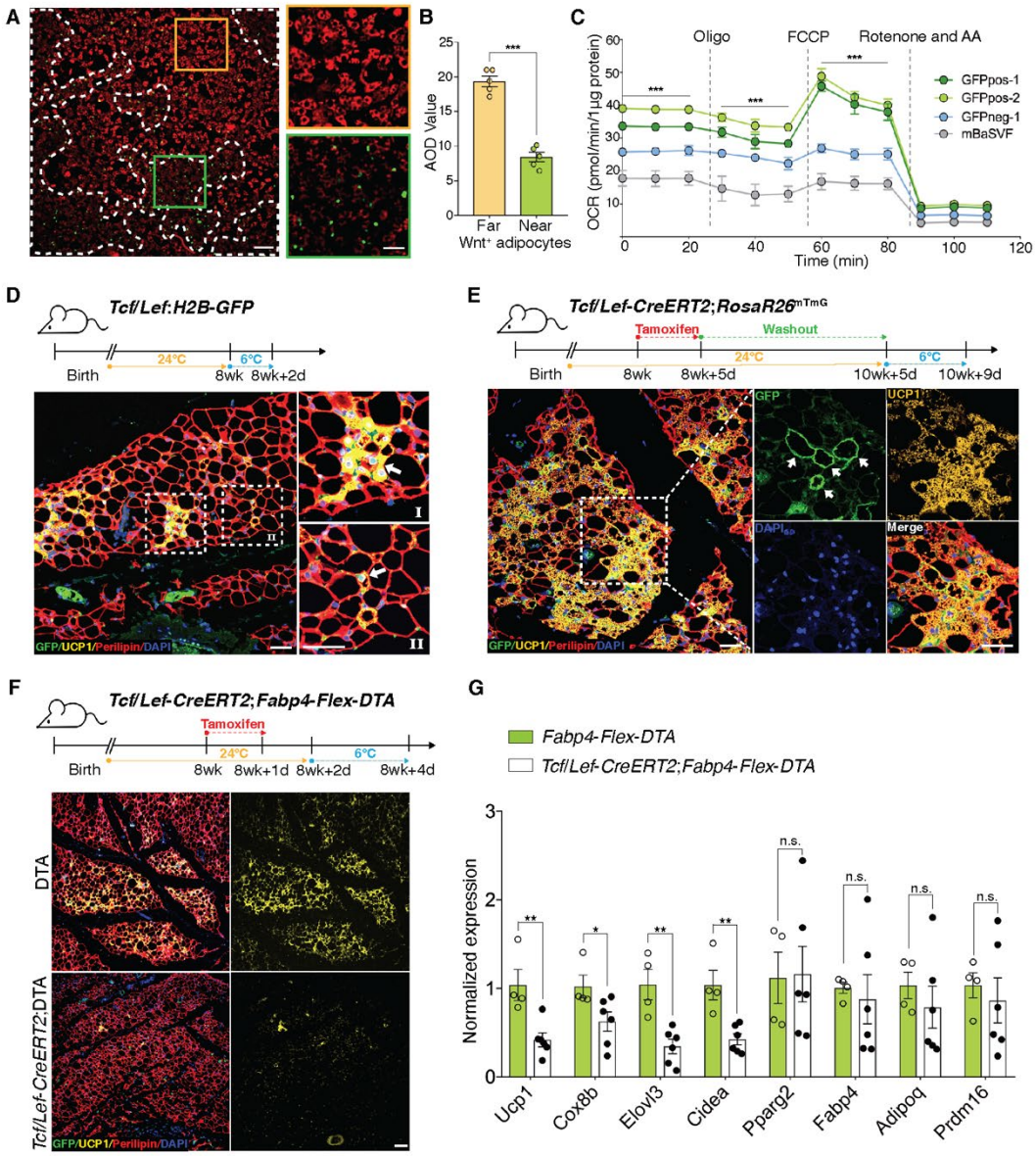

Fig. 4. Wnt⁺ adipocytes are essential for initiating adaptive thermogenesis. (**A**) Immunofluorescent staining of mitochondrial membrane potentials in Wnt⁺ adipocytes induced from iBAT-derived SVF cells of *T/L-GFP* mice. $n = 5$ independent experiments. Scale bar, 100 μm; close-up scale bar, 20 μm. (**B**) Quantification of staining in (A). Data are mean ± s.e.m., unpaired Student's *t*-test; ***$P < 0.001$. (**C**) OCR plots of four groups of adipocytes differentiated from GFPpos-1, GFPpos-2, GFPneg-1, and mBaSVF cell lines. $n = 3$ independent experiments. Data are mean ± s.e.m., two-way repeated ANOVA followed by Bonferroni's test; ***$P < 0.001$. (**D**) Immunofluorescent staining of iWAT from *T/L-GFP* mice after 2-day cold exposure. $n = 4$ mice. Scale bar, 50 μm; close-up scale bar, 20 μm. (**E**) Immunofluorescent staining of iWAT from tamoxifen-treated *Tcf/Lef-CreERT2*;*Rosa26R*^{mTmG} mice after 4-day cold exposure. $n = 8$ mice. Scale bar, 50 μm. (**F**) Immunofluorescent staining of iWAT from tamoxifen-treated *Tcf/Lef-CreERT2*;*Fabp4-Flex-DTA* mice after 2-day cold exposure. $n = 6$ mice. Scale bar, 50 μm. (**G**) qPCR analysis of gene expression in iWAT from control (*Fabp4-Flex-DTA*) and *Tcf/Lef-CreERT2*;*Fabp4-Flex-DTA* mice in (F). Data are mean ± s.e.m., unpaired Student's *t*-test; n = 4, 6 mice; *$P = 0.0485$; ** $P < 0.01$; ***$P < 0.001$; n.s., not significant.

Supplemental Figures

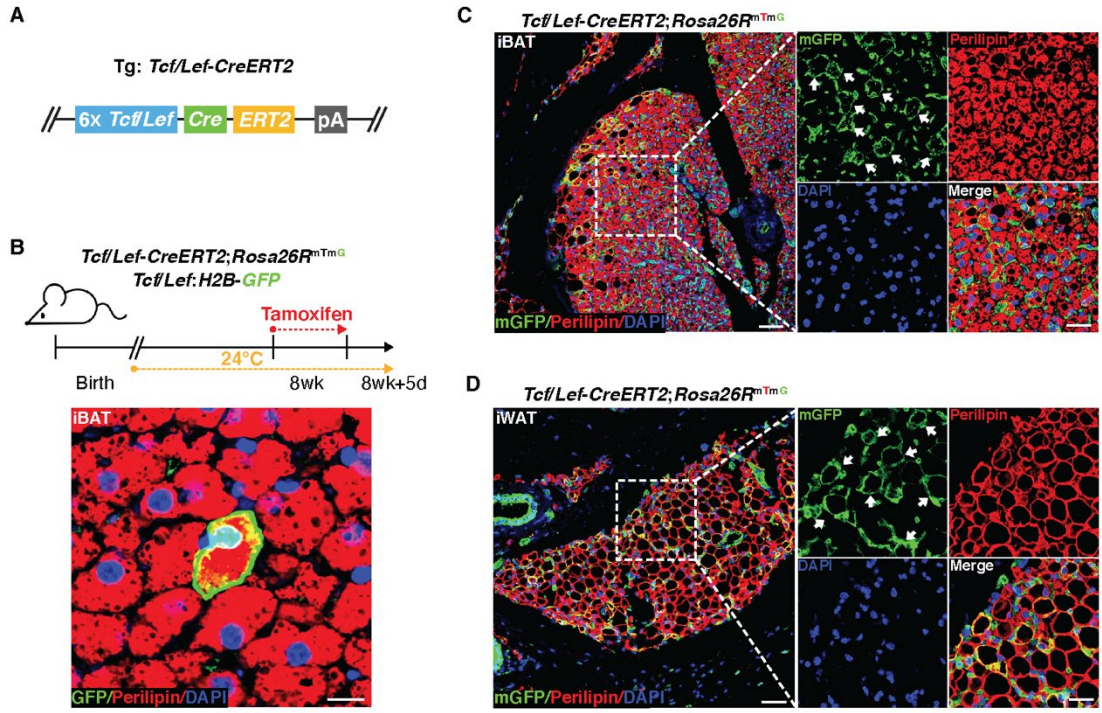

Supplemental Fig. 1. An inducible mouse model validates the existence of Wnt/β-catenin-positive adipocytes. (**A**) Schematic overview of the *TCF/Lef-CreERT2* allele. (**B**) GFP expression in the cell membrane and nucleus of an adipocyte in *Tcf/Lef-CreERT2*;*Rosa26R*^{mTmG};*T/L-GFP* mice. Scale bar, 10 μm. (**C** and **D**) *Tcf/Lef-CreERT2;Rosa26R*^{mTmG} mice exhibited mGFP-positive adipocytes (white arrows) in iBAT (C) and iWAT (D) after tamoxifen treatment. n = 4 mice each. Scale bars, 50 μm; close-up scale bars, 20 μm.

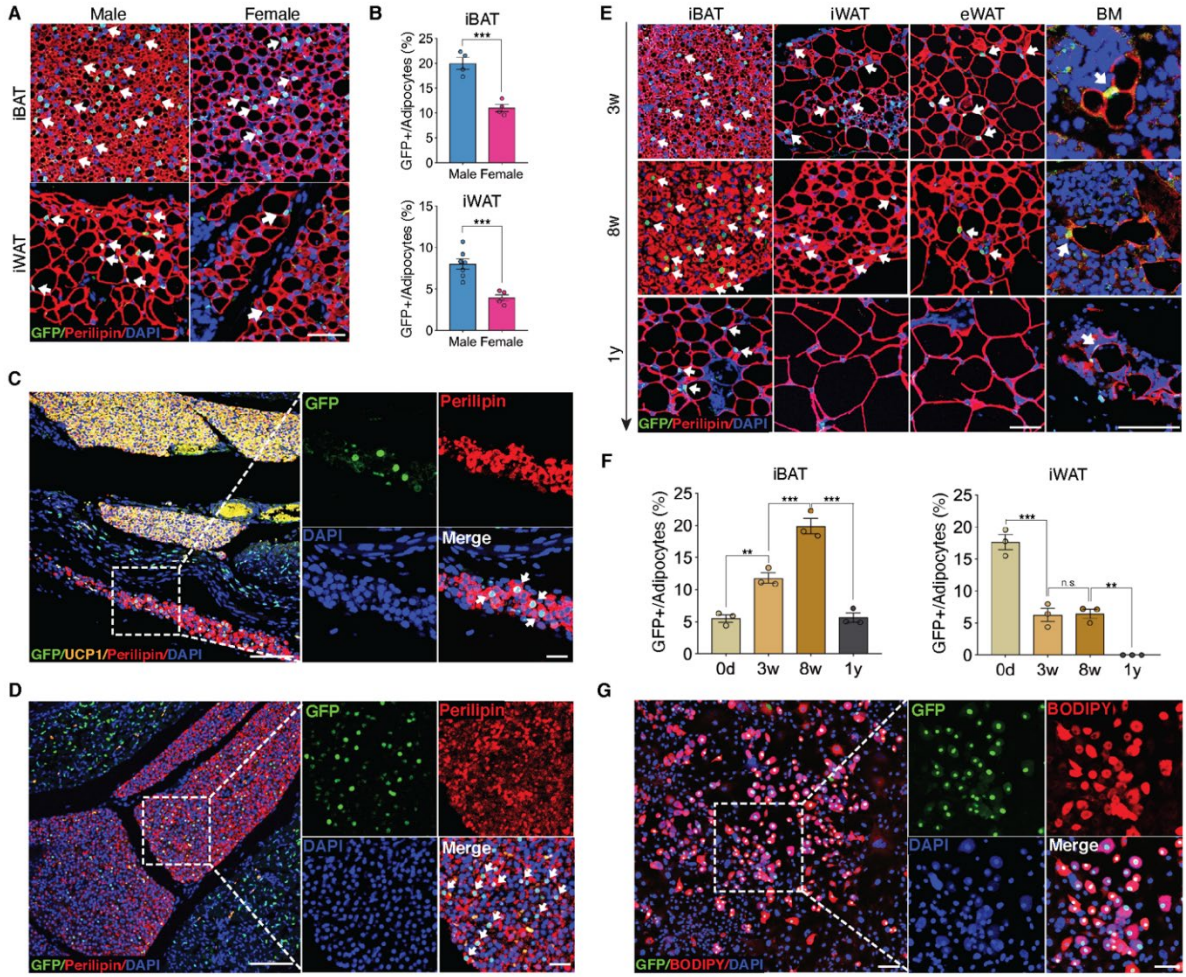

Supplemental Fig. 2. Age- and sex-dependent dynamics of Wnt$^+$ adipocytes. (**A**) Immunofluorescent images of iBAT and iWAT from adult male and female mice showing Wnt$^+$ adipocytes. n = 4-7 mice. Scale bar, 50 µm. (**B**) Quantification of Wnt$^+$ adipocytes among total adipocytes in (A). Data are mean ± s.e.m., unpaired Student's t-test; ***P < 0.001. (**C**) Immunofluorescent images of subcutaneous WAT adjacent to iBAT from E17.5 *T/L-GFP* mouse showing initial appearance of Wnt$^+$ adipocytes. n = 3 embryos. Scale bar, 100 µm; close-up scale bar, 25 µm. (**D**) Immunofluorescent images of iBAT from E18.5 *T/L-GFP* mice showing initial appearance of Wnt$^+$ adipocytes. n = 3 embryos. Scale bar, 100 µm; close-up scale bar, 25 µm. (**E**) Immunofluorescent images of various fat depots from *T/L-GFP* mice at different ages showing the presence of Wnt$^+$ adipocytes. n = 3 mice each. Scale bar, 50 µm. (**F**) Quantification of Wnt$^+$ adipocytes among total adipocytes in (E). Data are mean ± s.e.m., one-way ANOVA followed by Tukey's test; **P < 0.01; ***P < 0.001; n.s., not significant. (**G**) Immunofluorescent images of Wnt$^+$ adipocytes induced from E13.5 MEFs in vitro. n = 2 independent experiments from 8 embryonic mice, 3 independent wells each. Scale bar, 100 µm; close-up scale bar, 20 µm. White arrows in all panels point to Wnt$^+$ adipocytes.

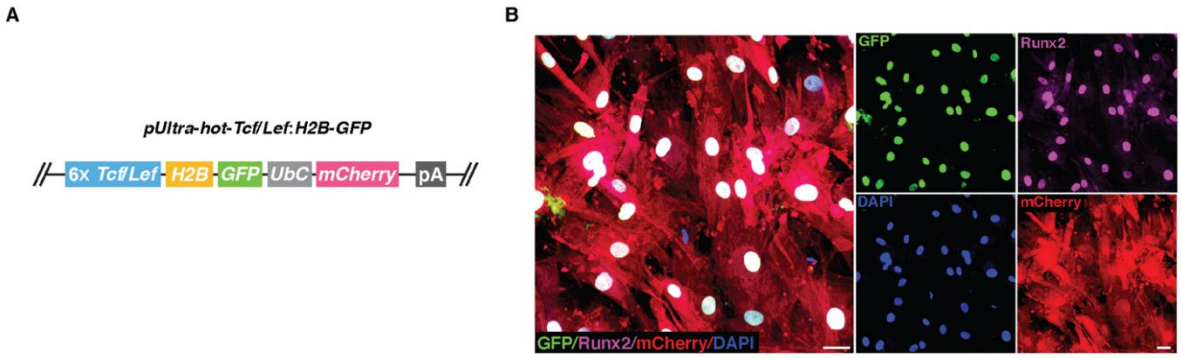

Supplemental Fig. 3. Infection of lentiviral virus in hBMSCs study. (**A**) Construct of the lentiviral shuttle vector. (**B**) Representative immunofluorescent images of infected hBMSCs in pro-osteogenic differentiation medium showing the expression of GFP in the nuclei of osteocytes, indicative of the activation of Wnt/β-catenin signaling. n = 2 independent experiments, 3-4 independent wells each. Scale bars, 50 μm.

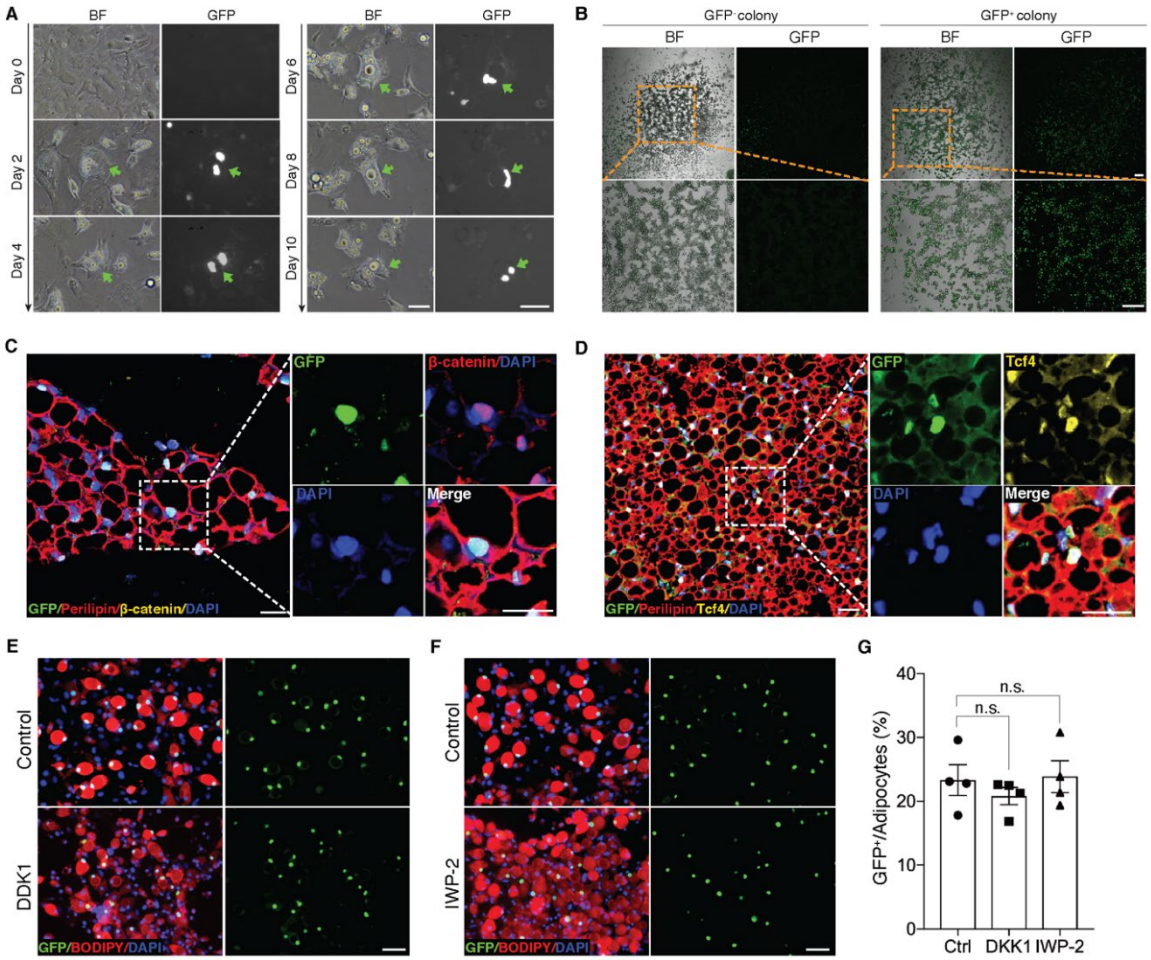

Supplemental Fig. 4. Wnt⁺ adipocytes with sustained Wnt/β-catenin signaling activity. (**A**) Real-time monitoring microscopy images of Wnt⁺ adipocytes during adipogenesis, which were induced from BMSCs of *T/L-GFP* mice. n = 3 independent experiments. Scale bar, 50 μm. (**B**) Microscopy images of GFP⁻ and GFP⁺ colonized adipocytes after 7-day differentiation induced from BMSCs of *T/L-GFP* mice. n = 4 independent experiments. Scale bar, 200 μm. (**C** and **D**) Immunofluorescent images of active β-catenin (C) and Tcf4 (D) in Wnt⁺ adipocytes. n = 3 mice each. Scale bars, 20 μm (C), 25 μm (D). (**E** and **F**) Immunofluorescent images of induced Wnt⁺ adipocytes from BMSCs of *T/L*-GFP mice treated with DKK1 (E) and IWP-2 (F). n = 4 independent experiments each. Scale bars, 50 μm. (**G**) Quantification of Wnt⁺ adipocytes among total adipocytes in (E) and (F). Data are mean ± s.e.m. and calculated by one-way ANOVA followed by Tukey's test. n.s., not significant.

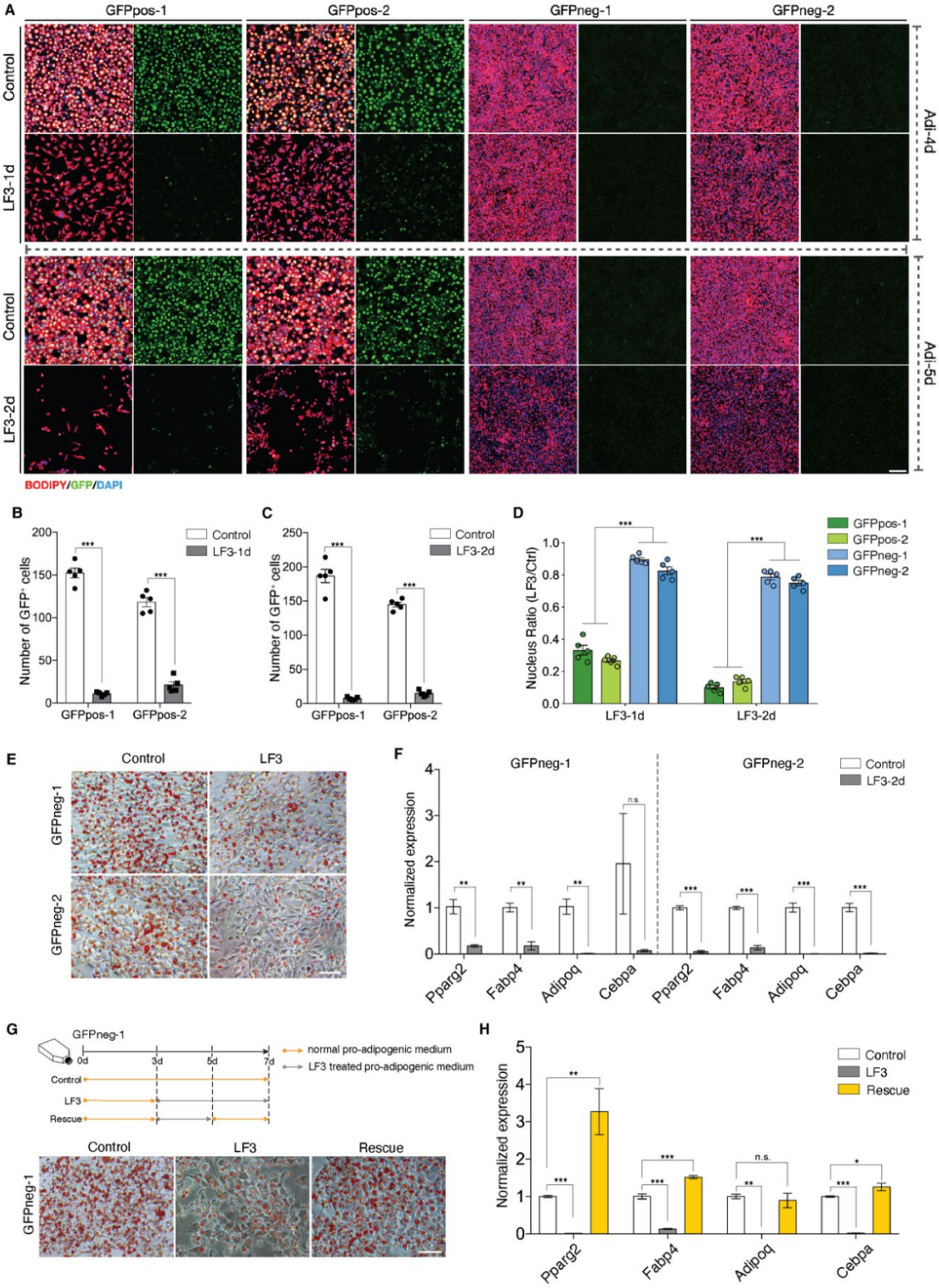

Supplemental Fig. 5. Wnt/β-catenin signaling is required for Wnt$^+$ adipocyte survival and Wnt$^-$ adipocyte maturation. (**A**) Immunofluorescent images of Wnt$^+$ and Wnt$^-$ adipocytes induced from four independent cell lines (GFPpos-1, -2 and GFPneg-1, -2) with LF3 treatment (50 μM) for one and two days, respectively. LF3 was added into the medium after 3-day pro-adipogenic induction. Note that by 1-day LF3 administration, GFP signals were significantly quenched in Wnt$^+$ adipocytes, along

with obviously reduced number. Wnt^- adipocytes began to show delayed adipogenic maturation. By 2-day LF3 administration, remarkable cell death of Wnt^+ adipocytes was seen and delayed adipogenic maturation in Wnt^- adipocytes became clear, compared to controls. Scale bar, 100 μm. (**B** and **C**) Quantification of Wnt^+ adipocyte number in (A). Data are mean ± s.e.m., unpaired Student's *t*-test; n = 5 independent experiments; ***P < 0.001. (**D**) Quantification of the nucleus ratio of LF3-treated adipocytes to control cells in (A). Data are mean ± s.e.m., one-way ANOVA followed by Tukey's test; n = 5 independent experiments; ***P < 0.001. DAPI was used as counter stain. (**E**) Microscopy images of Oil Red O staining in adipocytes induced from GFPneg-1 and -2 cell lines showing reduced lipid accumulation by LF3 treatment for two days. n = 3 independent experiments. Scale bar, 50 μm. (**F**) qPCR analysis of the expression of adipogenic genes in (E). Data are mean ± s.e.m., unpaired Student's *t*-test; **P < 0.01; ***P < 0.001; n.s., not significant. (**G**) Schematic of rescue experiment and microscopy images of Oil Red O staining in adipocytes induced from GFPneg-1 cell line with LF3 treatment. n = 3 independent experiments. Scale bar, 50 μm. (**H**) qPCR analysis of the expression of adipogenic genes in (G). Data are mean ± s.e.m., one-way ANOVA followed by Tukey's test; *P = 0.0460; **P < 0.01; ***P < 0.001; n.s., not significant.

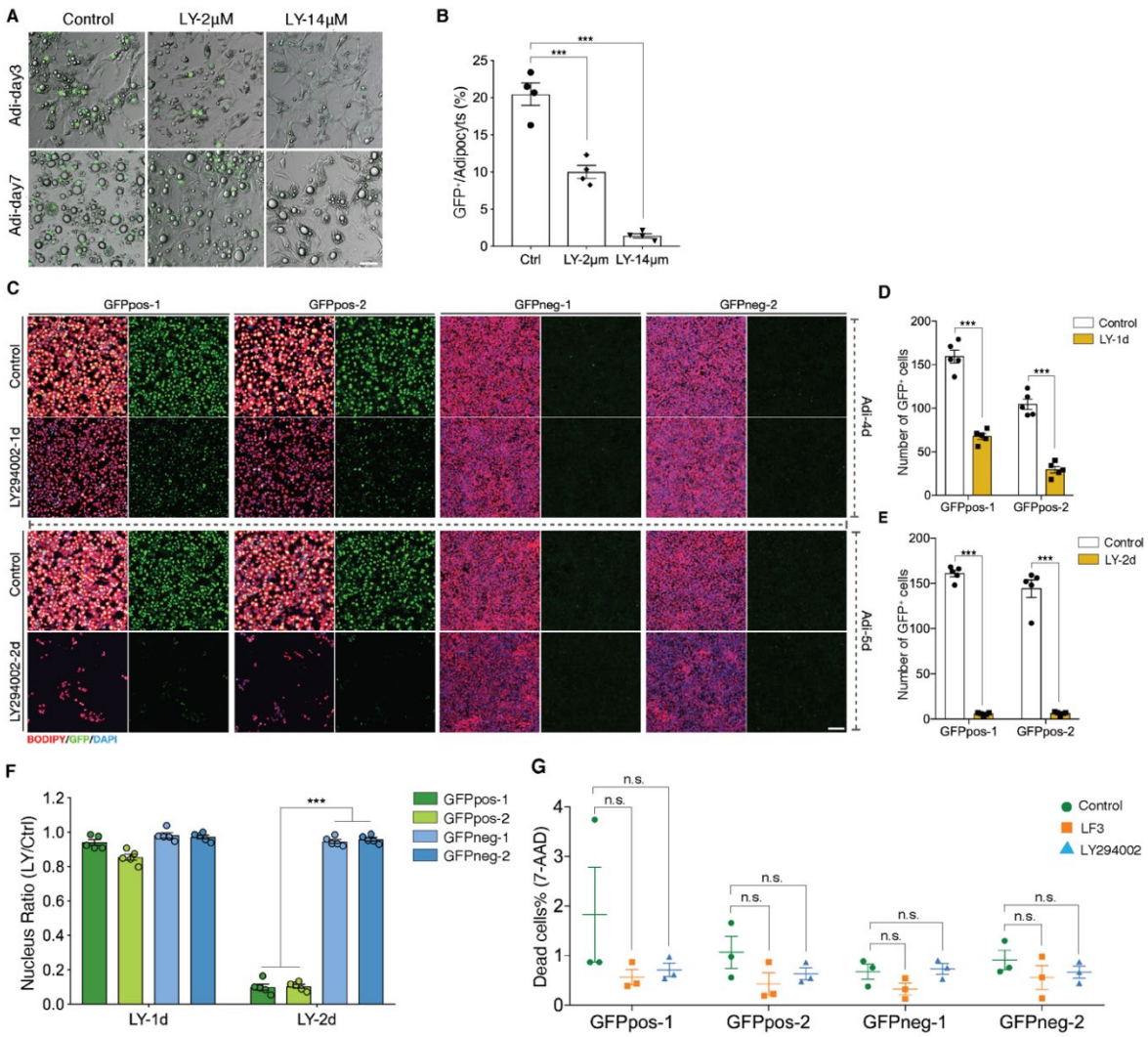

Supplemental Fig. 6. Inhibition of Akt signaling by LY294002 yields similar results as LF3 treatment. (**A**) Microscopy images of LY294002-treated adipocytes showing reduced number of Wnt$^+$ adipocytes and delayed adipogenesis after 3- and 7-day treatment compared to controls. $n = 4$ independent experiments. Scale bar, 20 μm. (**B**) Quantification of Wnt$^+$ adipocyte among total adipocytes after 7-day treatment in (A). Data are mean ± s.e.m., one-way ANOVA followed by Tukey's test; ***$P < 0.001$. (**C**) Immunofluorescent images of Wnt$^+$ and Wnt$^-$ adipocytes induced from four independent precursor cell lines (GFPpos-1, -2 and GFPneg-1, -2) with LY294002 treatment (14 μM) for one and two days, respectively. LY294002 was added into the medium after 3-day pro-adipogenic induction. LY294002 treatment diminished GFP signals prior to causing marked cell death in Wnt$^+$ adipocytes. In addition, LY294002 treatment also led to slightly reduced lipid storage in Wnt$^-$ adipocytes. $n = 5$ independent experiments. Scale bar, 100 μm. (**D** and **E**) Quantification of Wnt$^+$ adipocyte number in (C). Data are mean ± s.e.m., unpaired Student's *t*-test; ***$P < 0.001$. (**F**) Quantification of the nucleus ratio of LY294002-treated adipocytes to control cells in (C). Data are mean ± s.e.m., one-way ANOVA followed by Tukey's test; ***$P < 0.001$. DAPI was used as counter stain. (**G**) Quantification of the percentage of 7-AAD-positive cells by flow cytometry analyses showing comparable cell viability between LF3- or LY294002-treated immortalized cells and controls at the same doses. Data are mean ± s.e.m., one-way ANOVA followed by Tukey's test; $n = 3$ independent experiments; n.s., not significant.

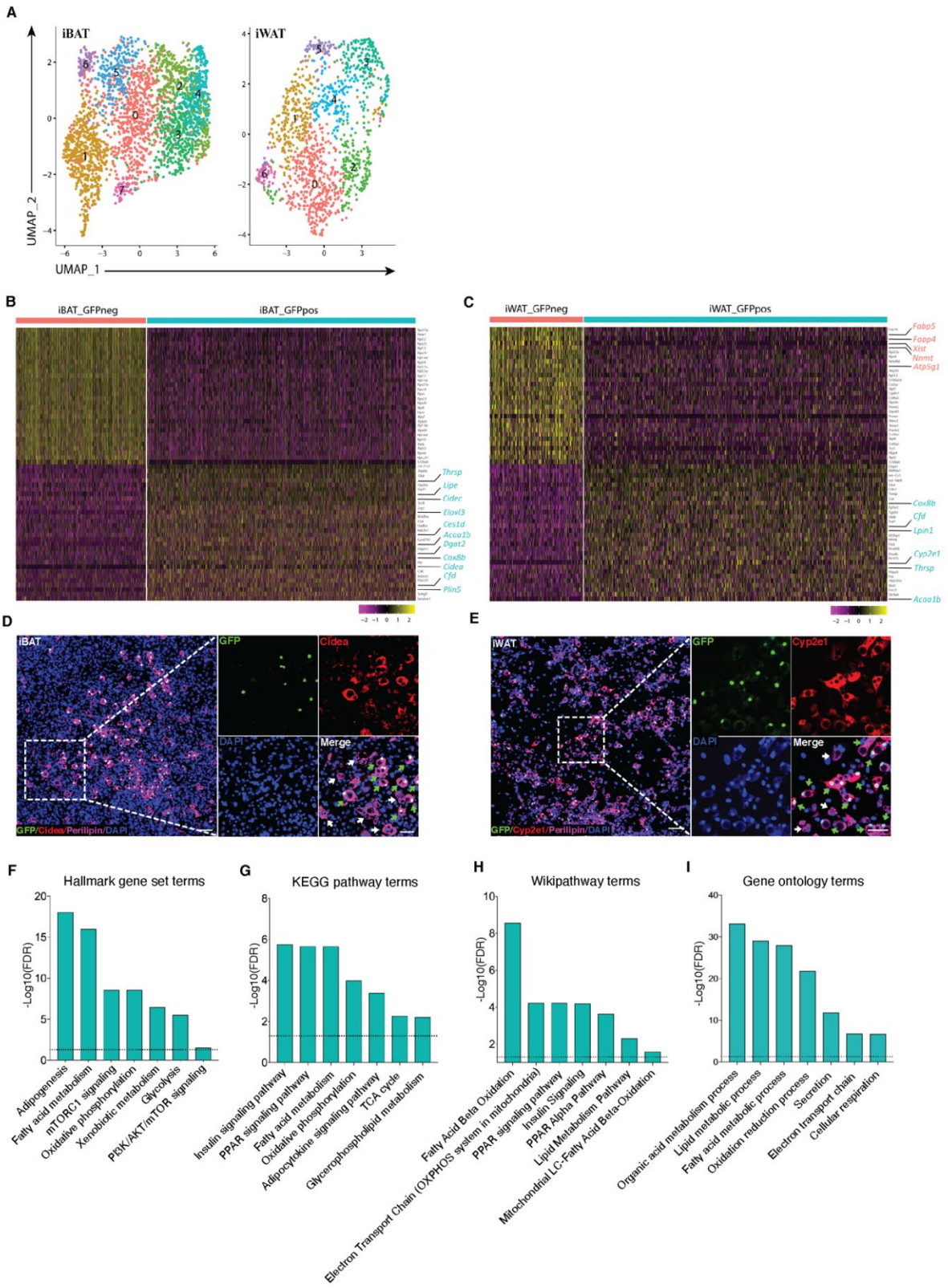

Supplemental Fig. 7. Wnt$^+$ adipocytes are distinct from Wnt$^-$ ones in molecular signatures. (**A**) UMAP visualization of unsupervised clustering in scRNA-seq. (**B** and **C**) Heat maps of expression of top 30 signature genes in iBAT- (B) and iWAT-derived (C) Wnt$^+$ and Wnt$^-$ adipocytes in scRNA-seq. (**D** and **E**) Immunofluorescent staining of Cidea in adipocytes induced from iBAT-derived SVFs (D) and Cyp2e1 in adipocytes induced from iWAT-derived SVFs (E). n = 3 independent experiments. Scale bars, 100 μm; close-up scale bars, 25 μm. (**F-I**) Hallmark gene sets (F), KEGG pathway (G),

1 Wikipathway (H), and GO Biological Processes ontology (I) analyses of DEGs enriched in iWAT-
2 derived Wnt^+ adipocytes in scRNA-seq.

Supplemental Fig. 8. Wnt$^+$ adipocytes are distinct from Wnt$^-$ ones in genomic signatures. (**A**) UMAP visualization of unsupervised clustering in scATAC-seq. (**B** and **C**) Enriched DNA motifs of iBAT- (B) and iWAT-derived (C) Wnt$^+$ (upper panels) and Wnt$^-$ (lower panels) adipocytes in scATAC-seq. (**D** and **E**) ScATAC-seq tracks of iBAT- (D) and iWAT-derived (E) Wnt$^+$ and Wnt$^-$ adipocytes showing distinct chromatin accessibilities of representative genes.

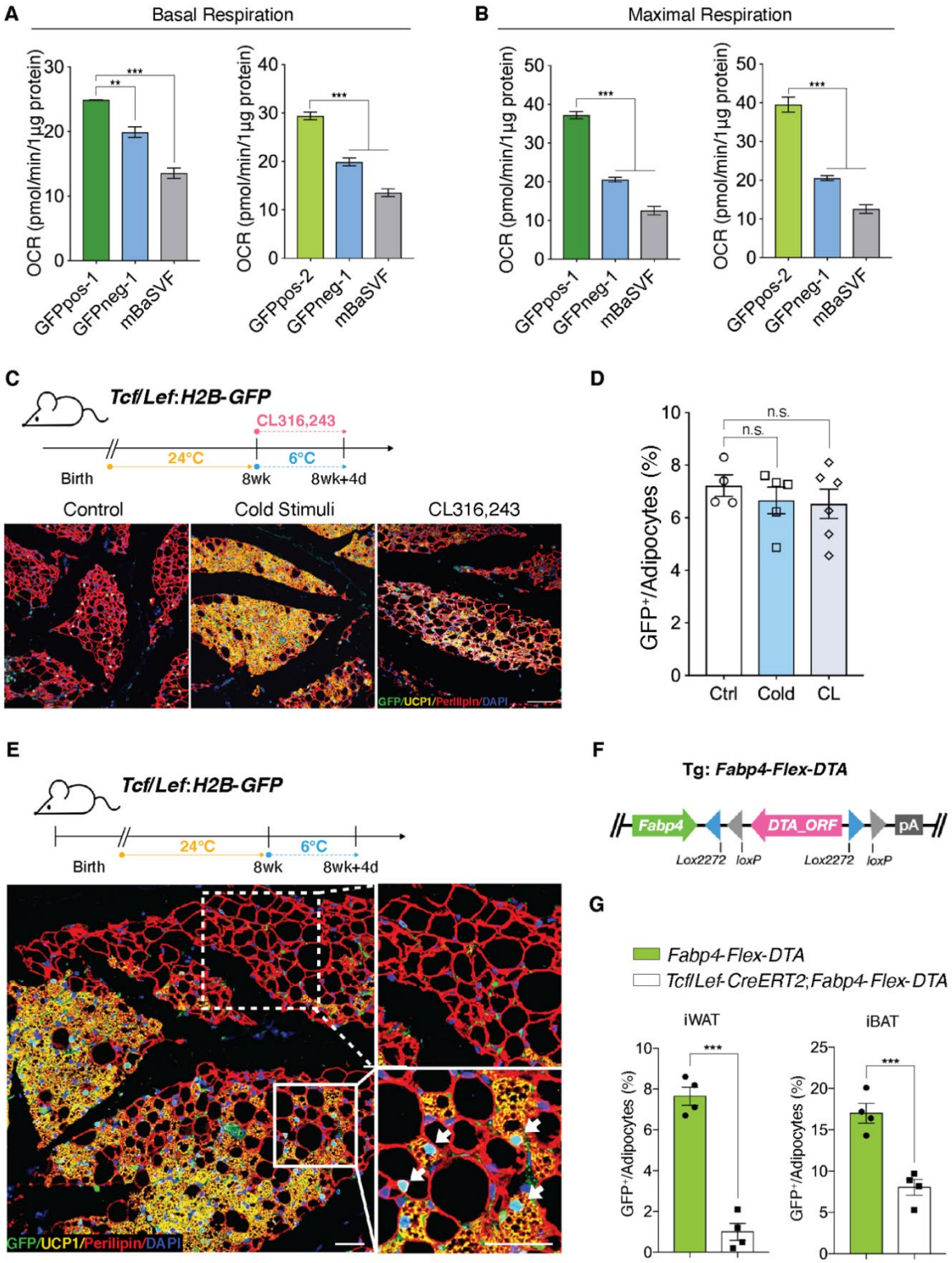

Supplemental Fig. 9. Wnt$^+$ adipocytes participate in adaptive thermogenesis in iWAT. (**A** and **B**) Calculated basal (A) and maximal (B) respiration levels in OCR assay in **Fig. 4C**. Data are mean ± s.e.m., one-way ANOVA followed by Tukey's test; $^{**}P = 0.0046$; $^{***}P < 0.001$. (**C**) Immunofluorescent images of iWAT from *T/L-GFP* mice after 4-day cold stress (n = 5 mice), CL316,243 treatment (n = 6 mice), and control (n = 4 mice). Scale bar, 100 µm. (**D**) Quantification of Wnt$^+$ adipocytes among total adipocytes in (C). Data are mean ± s.e.m., one-way ANOVA followed by Tukey's test; n.s., not significant. (**E**) Immunofluorescent images of iWAT from *T/L-GFP* mice with

4-day thermal challenge showing close association of Wnt^+ adipocytes with $UCP1^+$ beige adipocytes. *n* = 5 mice. Scale bars, 100 μm. (**F**) Schematic overview of the *Fabp4-Flex-DTA* allele. (**G**) Quantification of Wnt^+ adipocytes among total adipocytes of iWAT and iBAT from *Fabp4-Flex-DTA*;*T/L-GFP* and *Tcf/Lef-CreERT2*;*Fabp4-Flex-DTA*;*T/L-GFP* mice 24 hrs after one-time tamoxifen treatment prior to cold challenge. Data are mean ± s.e.m., unpaired Student's *t*-test; $n = 4$ mice each; ***$P < 0.001$.